Mesurement of A Remote Imaged Coronal Mass Ejection Driven Shock and Comparison with its signatures at 1 AU

Phillip Hess

School of Physics, Astronomy and Computational Sciences, George Mason University 4400 University Dr. Fairfax, VA 22030

phess4@gmu.edu

Jie Zhang

School of Physics, Astronomy and Computational Sciences, George Mason University 4400 University Dr. Fairfax, VA 22030

Received _____; accepted _____

1. Introduction

Coronal Mass Ejections (CMEs) and their counterpart at the Earth, Interplanetary Coronal Mass Ejections (ICMEs) are a major driver of space weather effects. A CME is an eruption of magnetized plasma from the Sun. Extreme cases of CMEs show speeds over 3000 km/s and carry as much as 10^{32} ergs of energy (Howard et al. 1985).

An ICME at the Earth will cause geomagnetic activity if its magnetic field has a strong component in the southern direction, making it oppositely aligned to the field of the Earth. This will cause magnetic reconnection along the magnetopause, opening the magnetospehere and allowing solar wind energy inside. These geomagentic storms can damage a wide array of technological systems, including satellites, power grids and GPS navigation systems as well as endangering astronauts in space. Therefore, being able to understand the processes governing CME evolution and predicting an arrival at the Earth are crucial to our increasingly technological society (Burlaga et al. 1987; Gosling et al. 1990).

Before the launch of the Solar Terrestrial Earth Observatory (STEREO) Mission in 2006, attempts to study CME evolution were limited to just two sets of data, near Sun white light observations from coronographs and in-situ solar wind observations near the Earth. The space in the heliosphere between these two regions was completely unobserved, making understanding of the evolution of CMEs difficult. However, STEREO changed this with the Sun Earth Connection Coronal and Heliosperic Investigation (SECCHI) suite of instruments, which provide a continuous view from the Sun to the Earth (Howard et al. 2008). Also, the STEREO mission is composed of two almost identical spacecraft in near Earth orbits around the Sun. This allows for stereoscopic imaging of the Sun. This, combined with SECCHI, allows the 3-dimensional tracking of CMEs all the way from the Sun to the Earth.

Many works have already been performed using SECCHI data to study the velocity of CMEs in the heliosphere (Wood & Howard 2009; Lugaz et al. 2009; Rouillard et al. 2009; Tappin & Howard 2009; Möstl et al. 2009; Liu et al. 2010). Most of these studies were performed by taking the position of the leading edge of the CME at different times to calculate a velocity. However, very few works have applied this same technique to the other front that can be associated with the CME, its driven shock front.

There are two different types of CMEs, fast and slow, that are differentiated by their initial velocities near the Sun (Sheeley et al. 1999). A slow CME will be slowly accelerated to the speed of the solar wind before the acceleration tapers off and becomes approximately constant. Fast CMEs are similar, as they begin with a velocity much higher than the solar wind and are decelerated toward the constant solar wind velocity. When A CME is sufficiently faster than the solar wind medium in which it travels, a driven shock wave can form.

In addition to the ICME at the Earth, geomagnetic storms can be caused by CME driven shock waves. A CME that is initially traveling much faster than ambient solar wind will produce a shock wave, which can open the magnetosphere with a southward magnetic field and have a significant space weather impact(Gosling et al. 1991). Therefore, just as understanding CME propagation is important to space weather, understanding the evolution of the shock is just as important. Fortunately, it has been shown before that in addition to having obvious structures in in-situ solar wind data, shocks of sufficient strength can also be seen in white light images (Maloney & Gallagher 2011; Bemporad & Mancuso 2010; Ontiveros & Vourlidas 2009; Vourlidas et al. 2003). It is then possible to use SECCHI to track both the CME and the shock it drives though the interplanetary space and relate it to in-situ signatures at the Earth.

Understanding shocks hass becoming vitally important, as in addition to causing

geomagnetic storms with a southward magnetic field, shocks are also known to accelerate energetic particles, which are among the most urgent space weather concerns. (Kahler & Reames 2003; Gopalswamy et al. 2002; Reames 1999). Shock measurements may also become more imporant as Kim et al. (2012) demonstrate a method of determining the magnetic field strength of a CME measurements of the CME shock.

To clear up confusion in the rest of the paper, the following are the terminology will be used to describe CME and ICME structure throughout the rest of this paper:

The ejecta front is the CME material that is actually ejected from the corona. The term flux rope will be used almost interchangeably with ejecta, as the ejecta front is assumed to be a flux rope during its propagation. In the classical ' three part' CME structure (Illing & Hundhausen 1985), this area is considered to be the cavity. The ejecta has a twisted magnetic field with a fairly low density. This low denisty makes imaging of the ejecta difficult, but by performing different methods of background subtraction, the ejecta can be seen in images.

The shock front is the outermost front seen in images. It is a shock wave caused by a very fast CME as it travels through the interplanetary space. In images it is seen as a faint and diffuse region in front of the ejecta.

In between these two fronts, the sheath region is an area of accumulated solar wind material in front of the ejecta that is highly dense and can contain a complicated magnetic structure.

ICME will hereafter only refer to CME signatures as seen in-stiu with the Advanced Composition Explorer (ACE) spacecraft. The different signatures that will be discussed are the shock, which is seen as a sharp increase in magnetic field strength, velocity and density (Jackson 1986); the sheath, a high density region between the shock and the flux rope; and

the classical flux rope signature, a rotating magnetic field (meaning that in the north-south direction the magnetic field direction goes from either positive to negative or negative to positive), a temperature that is significantly lower than expected based on the density, and a region where magnetic pressure is significantly larger than thermal pressure, (Zhang et al. 2008) which can also be considered a region of very low β.

Initially, the ejecta is relatively small and has its highest density, so it will be very bright in white light images. Conversely, the sheath will initially be very faint, as it is comprised of accumulated solar wind plasma in front of the CME. As the CME propagates, these brightness intensities will reverse relative to one another, as the CME will continue to expand as it propagates which will decrease its denisty but the shock will accumulate more and more plasma and will therefore gain brightness, or at least, lose brightness less quickly than the ejecta.

2. Methods

Despite the advantages in tracking Coronal Mass Ejections provided by STEREO, obtaining accurate measurements is difficult. Many different methods and models for extracting CME height data from STEREO have been developed (Tappin & Howard 2009; Lugaz et al. 2009; Thernisien et al. 2009; Liu et al. 2010). For the purpose of studying the evolution of the shock and CME ejecta fronts, two different methods were used.

The first of these methods is a forward modeling technique which uses the Graduated Cylindrical Shell, or croissant model, utilizing the Raytrace code developed by Thernisien et al. (2009, 2006) This model involves taking a cylindrical croissant and superimposing it upon images from multiple spacecraft at once, using six free parameters to best match the model to the images. These parameters include the direction of propagation (longitude

and latitude), the leading edge distance of the ejecta from the Sun, the half angle width of the shell, the tilt angle of the central axis orientation, and the ratio between the major and minor radius of the flux rope (aspect ratio). Making the assumption that the other five parameters are roughly constant as the CME propagates, the leading edge height can be used to determine a height profile of the CME with time. Performing a numerical derivative of this data can then yield a velocity. In addition to fitting the flux rope, a simplified model for measuring the shock height is also used. While the model does not match the shock nearly as well as the flux rope, it is still useful for providing a leading edge height. This height can be compared to the flux rope height to provide information about the sheath region in between the two fronts. A demonstration of the model is shown in Figure 1.

After deciding upon this model,there was still the issue of how to properly apply it to study the two distinct fronts of the CME. What is often seen in images, such as Figure 2 is a very highly structured region with various bright regions throughout. The front of this region, which can be seen directly going back to the Sun, is taken as the ejecta front in this work. In front of the flux rope is a faint, diffuse region which has a parabolic shape. The front of this region is taken to be the shock and the region itself is the sheath.

In order to use as much data as possible, images from not only both STEREO spacecraft were used, but also from the Large Angle Spectrometric Coronograph Experiment (LASCO) on the the Solar and Heliospheric Observatory (SOHO) spacecraft, a coronograph showing the view of the Sun from Earth (Brueckner et al. 1995). Figure 1 shows a the raytrace mesh overlayed on to images from coronographs on all three spacecraft.

While others have been successful using the Raytrace model to track CMEs (Nieves-Chinchilla et al. 2012; Poomvises et al. 2010; Thernisien et al. 2009), another method was sought as validation for the Raytrace measurements. Using so-called jmaps (Sheeley et al. 1999), which are stack plots along a given position angle from one spacecraft that provide

plots in terms of elongation angle vs. time, other height measurements were also taken. However, due to various observational effects (Howard & Tappin 2009; Lugaz et al. 2009; Rollett et al. 2012), getting heights in distance from the Sun from jmaps is not as easy as just converting the elongation angles to a distance. There are many different methods for deriving true distances. In this work, two were used.

Close to the Sun, primarily in the STEREO COR2 field of view (4-15 R_s) the fixed-φ method was used. This method gives distances based on the equation

$$R = D_{obs}\frac{sin(\varepsilon(t))}{sin(\varepsilon(t)+\varphi)} \tag{1}$$

where ε is the elongation angle of the object being tracked, as determined from the jmap and φ is the direction of propagation of the CME, relative to the observer and D_{obs} is the distance from the observer to the Sun. While most work in the past that has been done has attempted to fit the data to provide the best direction of propagation, this study is different in that the propagation direction from raytrace was used, allowing for a straight-forward calculation of leading edge distances. While using the same direction of propagation as raytrace could introduce bias in the jmap data, it should not be a significant issue because direction of propagation has a relatively small error in the raytrace method. The jmaps used along the leading edge position angle are presented in Figure 3.

Near the Sun, fixed-φ is fairly accurate. However, as distances increase to be further out into the heliosphere, this method introduces errors, over-estimating the distance of the leading front of an object. (For detailed discussion of this, see Rollett et al. (2012)) For this reason, another method of extracting distances from the jmap was used for data further from the Sun, the harmonic mean method given by

$$R = D_{obs}\frac{2sin(\varepsilon(t))}{1+sin(\varepsilon(t)+\varphi)} \tag{2}$$

This method, while similar to the fixed-φ method, includes a geometric correction to account for the over-estimation. Combing the two methods near and further away from the

Sun, one data set could be created for judging the CME height profile based on observations from just one spacecraft.

These methods solved the problems of how to convert measurements from jmap elongation angles into heights, but there was still the issue of how to interpret the jmap data for the purposes of studying the separate fronts of the CME. Rouillard (2011) relates bright features in jmap data to density enhancements in-situ, which makes practical physical sense because the higher the density of a region, the more light will be Thompson scattered and the brighter these areas will be in white light images. Therefore, following this logic the bright features in the white light images will be taken to be the sheath region, which will have the highest density. The shock front will be the leading edge of the bright feature in the jmap and the ejecta front will be the trailing edge.

In the coronograpth field of view, due to the fact that the CME is brighter than the shock, this assumption may be invalid, but due to the relatively small distance between the two fronts this should not be very significant. The HI-1 data is where the two fronts begin to separate themselves more distinctly, so this is the more important data and in the majority of the HI-1 data the sheath gains more optical significance.

While this general assumption of the fronts should be valid, there is one very significant possible issue that should be considered with this interpretation of jmap data. Jmaps are constructed using running difference images, meaning the previous image to the one currently being used is subtracted out to highlight the new features that emerge. In the case of the shock front, this should not matter much, as the shock front is generally traveling into an empty region of space and can be well seen in a running difference image. However, if the sheath region is larger than distance traveled by the shock front between two images, the shock region that gets subtracted out from the previous image will remove the back of the sheath and will leave a dark void. In a jmap it is possible that this void would be

interpreted as the the ejecta when it is actually an observational effect. This, in conjunction with the general errors of smoothing the data needed to construct a coherent jmap should be remembered when handling this data set. Between these issues and the fact that a jmap is only taking data from one vantage point as opposed to the three views in raytrace, the raytrace is considered the more accurate measurement, but all data sets are useful.

3. Results

Applying these methodologies to the April 03, 2010 CME, both the shock front and ejecta front were tracked. Extreme Ultraviolet Images and GOES X-Ray data show an eruption occurring around 10:00 UTC on April 03. The eruption was associated with a relatively small flare and occurred from NOAA active region 11059. The CME was well observed in both STEREO A and B, as well as SOHO LASCO, in the low corona. The CME could be clearly seen in STEREO A all the way to the Earth, into the STEREO HI-2 field of view. It was not as clear in STEREO B HI-2 due to the presence of the Milky Way in the background. This event was also studied in depth by others (Möstl et al. 2010; Liu et al. 2011).

The ICME was also observed in-situ by ACE as seen in Figure 4. The shock is seen as a spike in the Magnetic Field, Velocity and Density at 08:00 UTC on April 05, 2010. The sheath lasts for three and and half hours until 11:30 UTC and initially shows a very strongly southern magnetic field which is likely the cause of a small geomagnetic storm with a dst peak of -77 nT at 15:00 UTC on April 06. The ejecta front arrives at 11:30 UTC on April 05 and the ejecta as a whole lasts until 15:00 UTC on April 06. The initial magnetic field is pointed northward and rotates southward, while also presenting a low β and a low temperature.

To keep the raytrace data consistent, the only one of the six parameters that was altered from time step to time step was the height, the other five were held constant for each measurement. While this certainly introduces errors as the CME will change in time due to solar rotation and internal forces, the assumption that these changes are not significant over the short time frame (less than one day) for which the measurements were carried out. The five constant parameters are presented in Table 1. The jmaps used for measurement were taken along the same position angle as the leading edge of the CME, so that a direct comparison with the height profile from the raytrace method could be made.

The heights, velocities and accelerations for the raytrace data set are shown in Figure 5. The velocities from each of the data set show a basic general agreement, but as already explained the raytrace data is considered the most reliable. The velocity profiles in Figure 5 show the CME reaching a high initial speed before decreasing to a constant speed. This is also reinforced by the ACE data, which shows a comparable velocity to the constant velocity of the fronts in the plot. The initial velocities all show a general agreement (except for the completely unrealistic result from the B jmap which shows an initial velocity for the ejecta larger than that of the shock) of an initial velocity around 1200 km/s for the shock and 1100 km/s.

The height profiles from each method are shown in Figure 6 throught the HI-1 field of view. Each of the three independent data sets shows a good agreement in the the height profiles for both fronts. The velocities for the CME for each data set as calculated with a numerical derivative show the same basic trends. These velocities show a bit more variation from data set to data set than the height data, but many similarities can be observed. It is obvious that the CME reaches a maximum speed of well over 1000 km/s before declining to a speed between 800 and 900 km/s. These values make sense, as the total time between the eruption and the arrival of the ejecta at ACE is about 49.5 hours, yielding an average

velocity of 833 km/s.

In order to determine some of the basic parameters of the CME velocity profiles from each data set and to attempt to extrapolate an arrival at the Earth with a simple empirical formula, the velocity data was fit with an exponential of the form

$$v(t) = v_f + (v_i - v_f)e^{(-t/t_c)} \tag{3}$$

Where v is the velocity at a given time,v_i is the initial velocity of the CME, v_f is the final velocity of the CME and t_c is the e-folding time describing the takes for the CME to reach its final asymptotic velocity. The fitting parameters from each data set are given in Table 2.

The most important number to look at in Table 2 is the final velocity, which has an aggreement between the raytrace data and the the B data of a shock velocity over 800 km/s and an ejecta velocity over 700 km/s. The jmap A data is considerably lower. ACE shows an initial velocity for both fronts to be between 700 and 800 km/s. The difference in the velocities between the extrapolated shock and the measured shock could be due to the difference between the extrapolations being done for the leading edge and ACE measuring something closer to the flank of the CME.

Figure 7 shows the standoff distance, or the distance between the leading edge of the shock front and the leading edge of the ejecta front from the raytrace data set. Again this data set was chosen because it was considered the most reliable and accurate. For the first 60 solar radii at least, the increase in standoff distance increases in an apparently linear fashion. To see if this linear evolution was possible, the standoff distance was fit with a line that was extrapolated out to 1 AU and compared to the observed sheath size at ACE, as calculated by taking the duration and velocity of the sheath. The extrapolated linear sheath would have been approximately 18 R_{Sun}, which is much larger than the calculated observation of approximately 13 R_{Sun}. If the calculated standoff distance within 60 R_{Sun} is believed, it cannot continue to increase at the same rate. An exponential fit, being applied

to the same data would match this leveling off of the standoff distance and also make sense given the assumption of exponential behavior in the velocity profile of the CME and shock. The exponential fit yielded a approximately 15 R_{Sun} standoff distance, much closer to the in-situ data. It should also be noted that comparing the standoff distance as measured from STEREO and in-situ data is not a direct 1:1 comparison, as the Raytrace measurements are along the CME leading edge and the in-situ data is of whatever part of the CME strikes the Earth.

4. Discussion and Conclusions

While too much cannot be determined from one single event, the results from the April 03 event did provide several encouraging results. The correlation for each front in both the raytrace and jmap methods from each satellite indicates that the methods are reasonably accurate for carrying out CME measurements. Besides matching each other, the measured height and derived velocity profiles are similar to the previously mentioned studies of the same event.

In addition to the agreement between different methods of measurement, the results also make sense because the velocity profiles produces match with known theories of fast CMEs that begin travelling extremely quickly before slowing down to a near constant speed.

Another test of the data that was performed was an extrapolation of the fits to 1 AU, in order to generate an arrival time that could be compared to the observed arrival at ACE. However, as previously mentioned, the data being used is not measuring the same part of the CME as ACE. The propagation direction of the CME as measured in raytrace was about 27 deg from the Sun-Earth line. It is difficult to know how much of a difference this will cause, as the front of the CME undergoes a very complex geometric evolution as it

propagates.

It is still worth comparing the predicted arrival times to the ACE data, as even with the aforementioned errors the prediction should be close, even with this simple empirical model. Figure 8 shows different predictions, based on different subsets of the data from both the raytrace measured data and the data from jmap A all the way out to the Earth. The jmap B data was not used, since the HI-2 data does not clearly show the event. The different arrival times are presented in Table 3. This is to see if accurate predictions are possible using only a small amount of data near the Sun. The predictions were generated by taking fits on the velocity data and integrating the fits to get position as a function of time. These functions were then solved in order to determine the time of the CME at 1 AU.

The different arrival times predicted for the shock especially are all encouraging, but all are within a few hours, even using data just a quarter of the way from the Sun to the Earth. However, since it is just one event the accuracy of this prediction method is still far from confirmed. It is encouraging though that this simple empirical formula was able to generate such accurate predictions for any event, especially with such a small subset of the data. In the future, more events must be studied in order to test subset of the data this method further.

In general, the methods used in this work show promise, but before any definitive conclusions can be drawn, more events must be studied in great detail. Future plans call for a catalog of events that display clear shock signatures at the Earth and can be studied in the same way as the April 03, 2010 event to provide a validation of the methods. Finding CMEs that work as well as the April 03 CME will not be trivial, as this CME was both directed very near the Earth and propagated in the interplanetary space free of any noticeable interaction with any other transient structures.

In addition to applying the same methods to other events, other planned work involves

using the equations from Maloney & Gallagher (2011) based on those put forth by Farris & Russell (1994) which will relate the standoff distance to the Mach number and the CME radius of curvature. We feel that the techniques presented in this work will be able to yield a meaningful exploration of the evolution of the CME front as it evolves in the heliosphere.

REFERENCES

Bemporad, A. & Mancuso, S. 2010, ApJ, 720, 130

Brueckner, G. E., Howard, R. A., Koomen, M. J., Korendyke, C. M., Michels, D. J., Moses, J. D., Socker, D. G., Dere, K. P., Lamy, P. L., Llebaria, A., Bout, M. V., Schwenn, R., Simnett, G. M., Bedford, D. K., & Eyles, C. J. 1995, Sol. Phys., 162, 357

Burlaga, L. F., Behannon, K. W., & Klein, L. W. 1987, J. Geophys. Res., 92, 5725

Farris, M. H. & Russell, C. T. 1994, J. Geophys. Res., 99, 17681

Gopalswamy, N., Yashiro, S., Michalek, G., Kaiser, M. L., Howard, R. A., Reames, D. V., & Leske, R.and von Rosenvinge, T. 2002, Astrophys. J., 572, L103

Gosling, J. T., Bame, S. J., McComas, D. J., & Phillips, J. L. 1990, Geophys. Res. Lett., 17, 901

Gosling, J. T., McComas, D. J., Phillips, J. L., & Bame, S. J. 1991, J. Geophys. Res., 96, 7831

Howard, R. A., Moses, J. D., Vourlidas, A., Newmark, J. S., Socker, D. G., Plunkett, S. P., Korendyke, C. M., Cook, J. W., Hurley, A., Davila, J. M., Thompson, W. T., St Cyr, O. C., Mentzell, E., Mehalick, K., Lemen, J. R., Wuelser, J. P., Duncan, D. W., Tarbell, T. D., Wolfson, C. J., Moore, A., Harrison, R. A., Waltham, N. R., Lang, J., Davis, C. J., Eyles, C. J., Mapson-Menard, H., Simnett, G. M., Halain, J. P., Defise, J. M., Mazy, E., Rochus, P., Mercier, R., Ravet, M. F., Delmotte, F., Auchere, F., Delaboudiniere, J. P., Bothmer, V., Deutsch, W., Wang, D., Rich, N., Cooper, S., Stephens, V., Maahs, G., Baugh, R., McMullin, D., & Carter, T. 2008, Space Sci. Rev., 136, 67

Howard, R. A., Sheeley, Jr., N. R., Koomen, M. J., & Michels, D. J. 1985, J. Geophys. Res., 90, 8173

Howard, T. A. & Tappin, S. J. 2009, Space Sci. Rev., 147, 31

Illing, R. M. E. & Hundhausen, A. J. 1985, J. Geophys. Res., 90(A1), 275

Jackson, B. V. 1986, Advances in Space Research, 6, 307

Kahler, S. W. & Reames, D. V. 2003, Astrophys. J., 584, 1063

Kim, R.-S., Gopalswamy, N., Moon, Y.-J., Cho, K.-S., & Yashiro, S. 2012, ApJ, 746, 118

Liu, Y., Davies, J. A., Luhmann, J. G., Vourlidas, A., Bale, S. D., & Lin, R. P. 2010, ApJ, 710, L82

Liu, Y., Luhmann, J. G., Bale, S. D., & Lin, R. P. 2011, ApJ, 734, 84

Lugaz, N., Vourlidas, A., & Roussev, I. I. 2009, Annales Geophysicae, 27, 3479

Maloney, S. A. & Gallagher, P. T. 2011, ApJ, 736, L5

Möstl, C., Farrugia, C. J., Temmer, M., Miklenic, C., Veronig, A. M., Galvin, A. B., Leitner, M., & Biernat, H. K. 2009, ApJ, 705, L180

Möstl, C., Temmer, M., Rollett, T., Farrugia, C. J., Liu, Y., Veronig, A. M., Leitner, M., Galvin, A. B., & Biernat, H. K. 2010, Geophys. Res. Lett., 37, 24103

Nieves-Chinchilla, T., Colaninno, R., Vourlidas, A., Szabo, A., Lepping, R. P., Boardsen, S. A., Anderson, B. J., & Korth, H. 2012, Journal of Geophysical Research (Space Physics), 117, 6106

Ontiveros, V. & Vourlidas, A. 2009, ApJ, 693, 267

Poomvises, W., Zhang, J., & Olmedo, O. 2010, ApJ, 717, L159

Reames, D. V. 1999, Space Sci. Rev., 90, 413

Rollett, T., Möstl, C., Temmer, M., Veronig, A. M., Farrugia, C. J., & Biernat, H. K. 2012, Sol. Phys., 276, 293

Rouillard, A. P. 2011, Journal of Atmospheric and Solar-Terrestrial Physics, 73, 1201

Rouillard, A. P., Davies, J. A., Forsyth, R. J., Savani, N. P., Sheeley, N. R., Thernisien, A., Zhang, T.-L., Howard, R. A., Anderson, B., Carr, C. M., Tsang, S., Lockwood, M., Davis, C. J., Harrison, R. A., Bewsher, D., Fränz, M., Crothers, S. R., Eyles, C. J., Brown, D. S., Whittaker, I., Hapgood, M., Coates, A. J., Jones, G. H., Grande, M., Frahm, R. A., & Winningham, J. D. 2009, Journal of Geophysical Research (Space Physics), 114, 7106

Sheeley, N. R., Walters, J. H., Wang, Y.-M., & Howard, R. A. 1999, J. Geophys. Res., 104, 24739

Tappin, S. J. & Howard, T. A. 2009, Space Sci. Rev., 147, 55

Thernisien, A., Vourlidas, A., & Howard, R. A. 2009, Sol. Phys., 256, 111

Thernisien, A. F. R., Howard, R. A., & Vourlidas, A. 2006, ApJ, 652, 763

Vourlidas, A., Wu, S. T., Wang, A. H., Subramanian, P., & Howard, R. A. 2003, ApJ, 598, 1392

Wood, B. E. & Howard, R. A. 2009, ApJ, 702, 901

Zhang, J., Poomvises, W., & Richardson, I. G. 2008, Geophys. Res. Lett., 35, 2109

Parameter	Value
Latitude	-26.2728 °
Longitude	260.785 °
Tilt Angle	14.535 °
Aspect Ratio	0.378943
Half Angle	24.9751 °

Table 1: The parameters used for the raytrace measurements. Latitude and Longitude are in Heliograpic Coordinate System, with Carrington Longitude.

Parameter	Raytrace Shock	Raytrace Ejecta	Jmap A Shock	Jmap A Ejecta	Jmap B Shock	Jmap B Ejecta
$V_i(km/s)$	1210.2	1101.6	1238.1	1158.4	1221.8	1278.6
$V_f(km/s)$	835.9	730.8	768.4	626.6	862.1	776.8
$T_c(hrs)$	1.38	1.96	3.93	4.61	3.41	2.44

Table 2: The values of the terms in teh exponential fitting for both fronts in each data set

	ACE	Raytrace ($28R_{Sun}$)	Raytrace ($36R_{Sun}$)	Raytrace ($55R_{Sun}$)	Jmap A All Data	Jmap A Half HI-2	Jmap A HI-1 only
Shock	08:00:00	10:24:14	13:17:18	04:55:58	05:25:06	03:45:34	04:00:30
Ejecta	11:30:00	17:16:14	22:31:58	07:16:46	12:17:34	09:16:14	05:57:50

Table 3: The actual arrival time given by ACE as well as predicted values from different subsets. For raytrace data numbers given are the last measurement used in the fitting. For the jmap data, subsets are given based om the amount of HI-2 data incorporated.

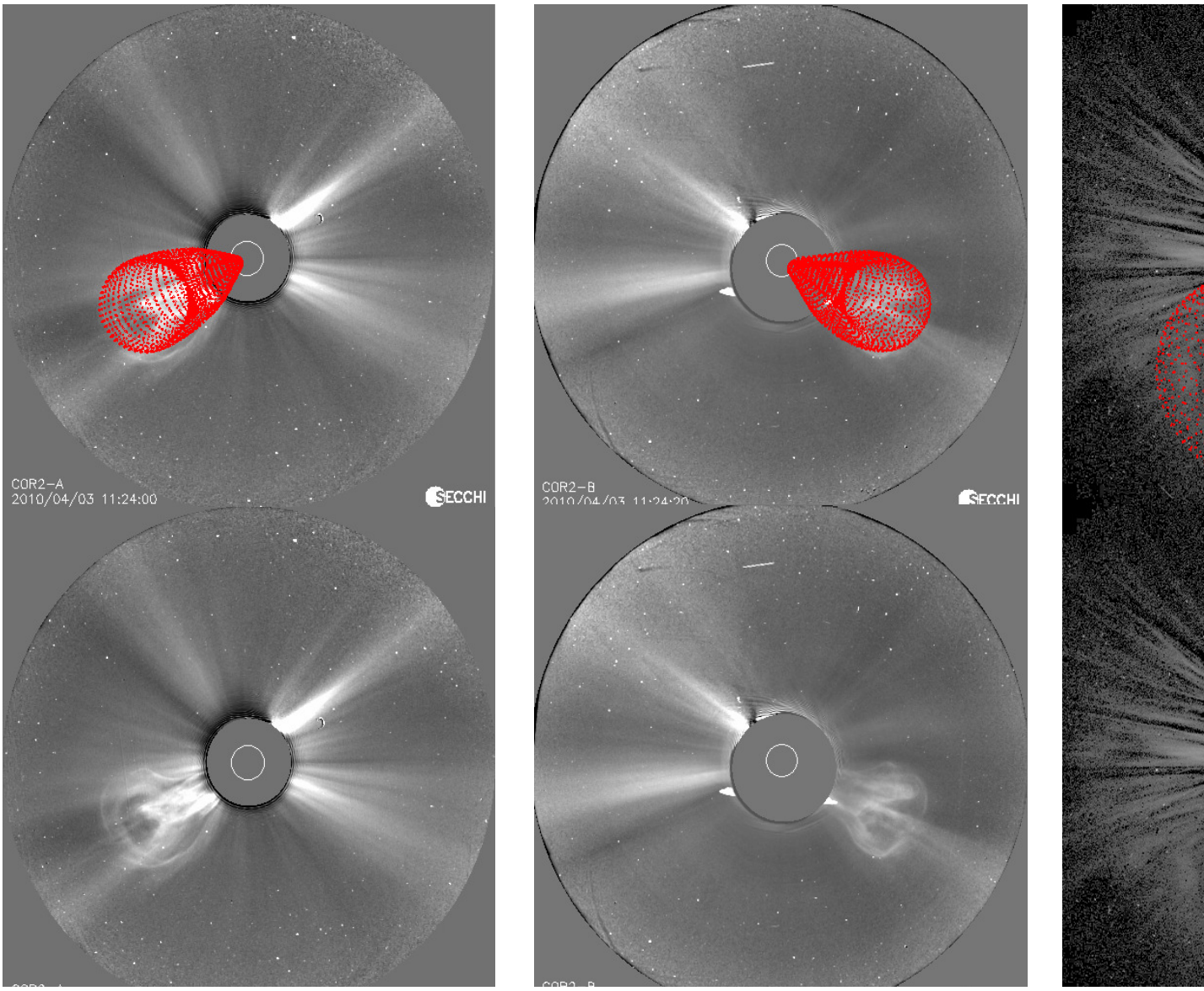

Fig. 1.— Images from STEREO A COR2 (Left), STEREO B COR2 (Center) and SOHO LASCO C2 (Right) with (top) and without (bottom) the raytrace mesh, demonstrating the way in which the method is used to match the GCS model to the white light images.

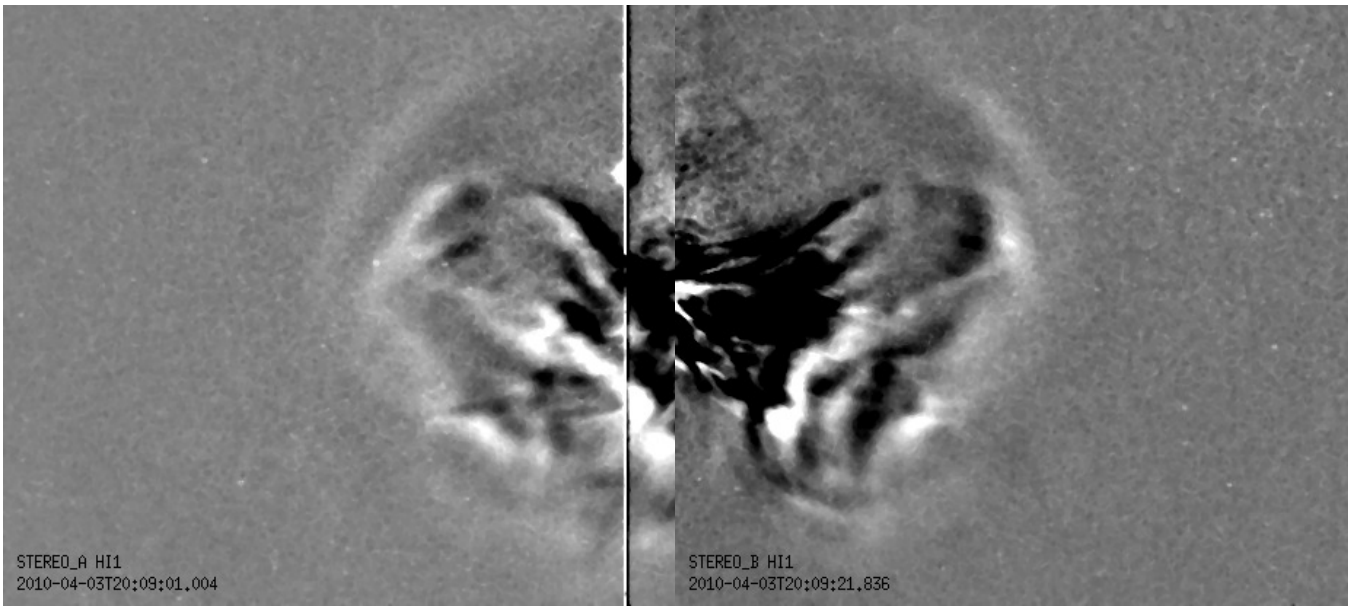

Fig. 2.— The April 03, 2010 CME in STEREO HI_1 field of view, both A (left) and B (right). In both spacecraft the the CME ejecta be seen as the bright, structured front. The sheath is the faint, diffuse region in front of it and the front of the sheath is the shock front

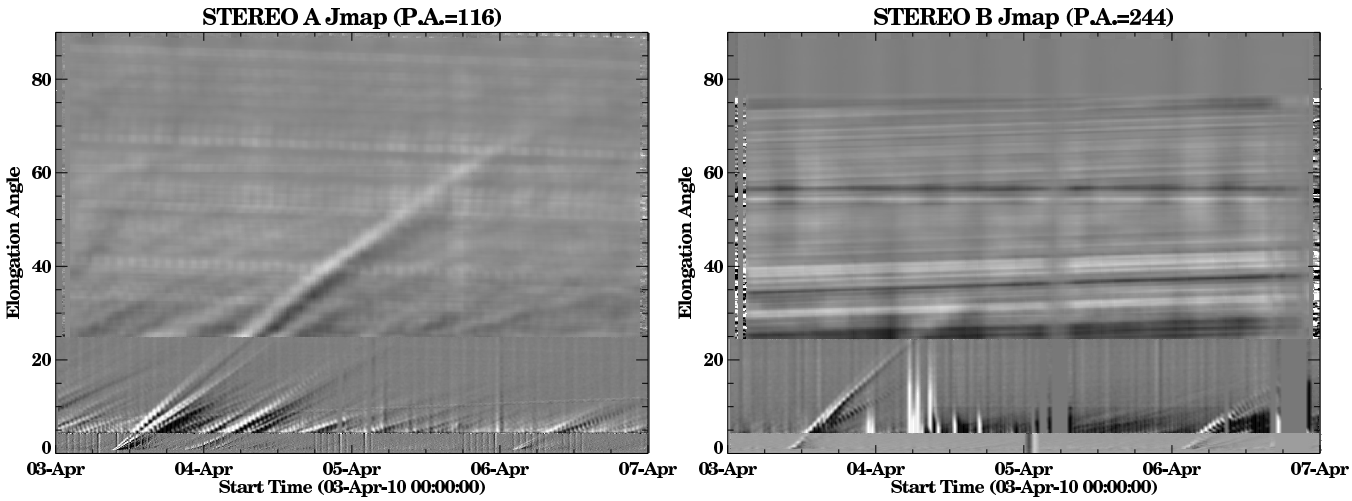

Fig. 3.— Jmaps of the April 03, 2010 CME for each STEREO spacecraft along the propagation angle as measured by raytrace. The CME is much clearer in STEREO A. The bright density enhancement is considered the sheath region of high density. The edge leading this sheath is the shock front and the trailing edge the CME Ejecta

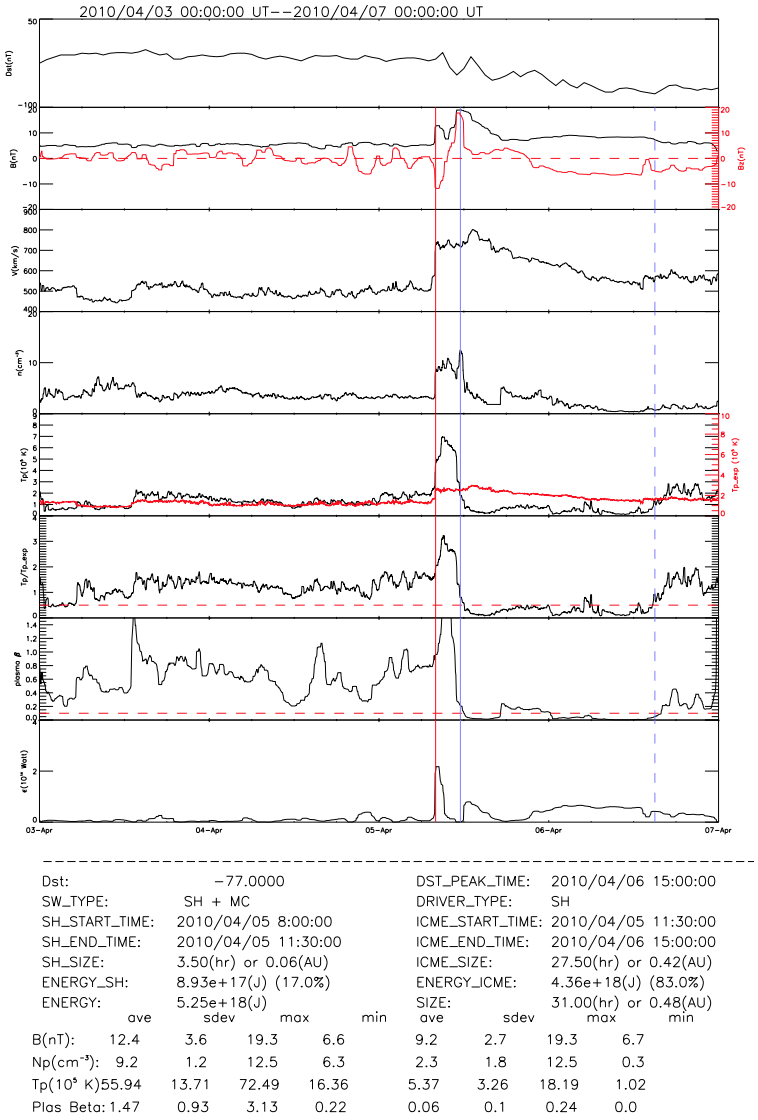

Dst:	−77.0000				DST_PEAK_TIME:	2010/04/06 15:00:00			
SW_TYPE:	SH + MC				DRIVER_TYPE:	SH			
SH_START_TIME:	2010/04/05 8:00:00				ICME_START_TIME:	2010/04/05 11:30:00			
SH_END_TIME:	2010/04/05 11:30:00				ICME_END_TIME:	2010/04/06 15:00:00			
SH_SIZE:	3.50(hr) or 0.06(AU)				ICME_SIZE:	27.50(hr) or 0.42(AU)			
ENERGY_SH:	8.93e+17(J) (17.0%)				ENERGY_ICME:	4.36e+18(J) (83.0%)			
ENERGY:	5.25e+18(J)				SIZE:	31.00(hr) or 0.48(AU)			
	ave	sdev	max	min		ave	sdev	max	min
B(nT):	12.4	3.6	19.3	6.6		9.2	2.7	19.3	6.7
Np(cm⁻³):	9.2	1.2	12.5	6.3		2.3	1.8	12.5	0.3
Tp(10⁵ K)	55.94	13.71	72.49	16.36		5.37	3.26	18.19	1.02
Plas Beta:	1.47	0.93	3.13	0.22		0.06	0.1	0.24	0.0

Fig. 4.— Solar Wind data measured by ACE between April 03 and April 07, 2010. The shock onset is denoted with the red line, the ejecta onset with the solid blue line and the passing of the ejecta with the dotted blue line. Plots from top to bottom show the Dst index, Total Magnetic Field and The z component of the magnetic field, total velocity, Density, The temperature and the expected temperature based on the density, the ratio between the two temperatures, the plasma *beta* and the total energy.

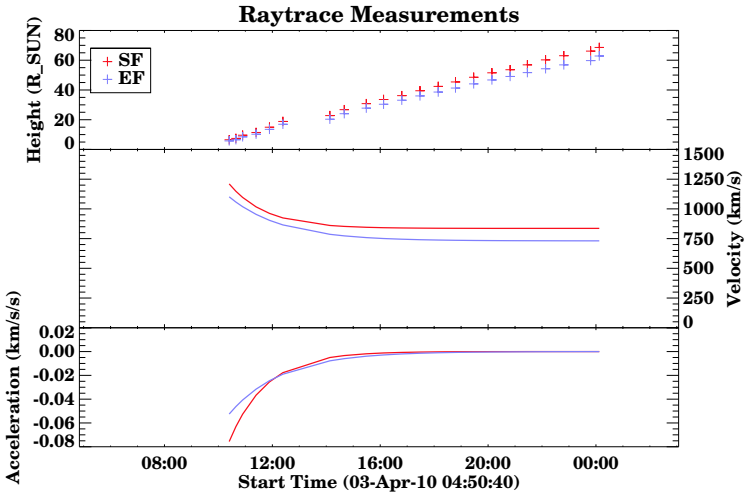

Fig. 5.— The top plot is the raytrace data showing the measured heights for both the shock (red) and ejecta (blue) fronts. The middle plot is the velocity fit of the derivative of the measurements and the botttom plot is the derivative of the velocity fit giving the acceleration of each front.

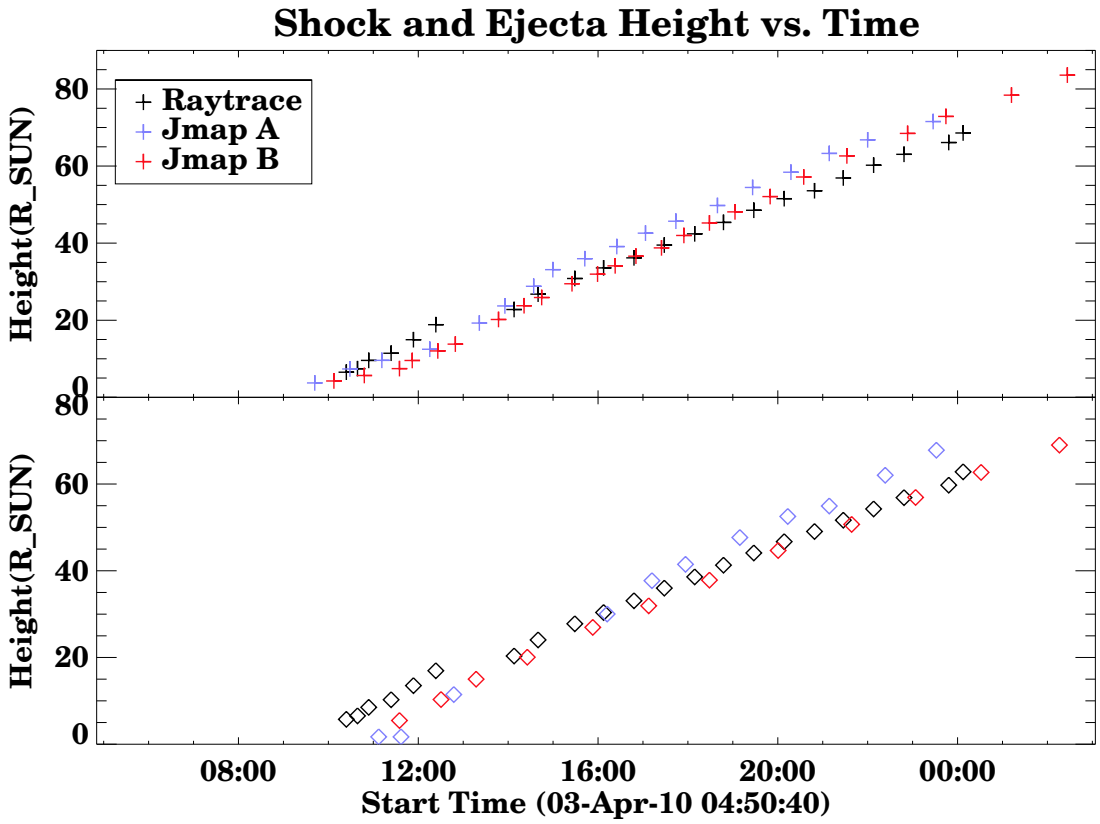

Fig. 6.— The measured height from each data set for both the shock (top, crosses) and the ejecta (bottom, diamonds) fronts. Black denotes raytrace, blue denotes the jmap from STEREO A and red denotes the jmap from STEREO B.

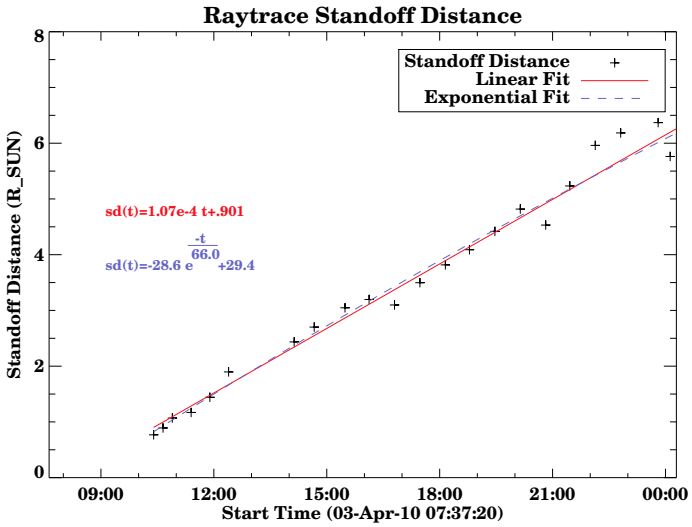

Fig. 7.— The standoff distance (black crosses), calculated by subtracting the measured ejecta front from the measured shock front. The red line is a linear fit of the standoff distance data and the blue dashed line is an exponential fit. The formulas for both fronts are shown on the plot.

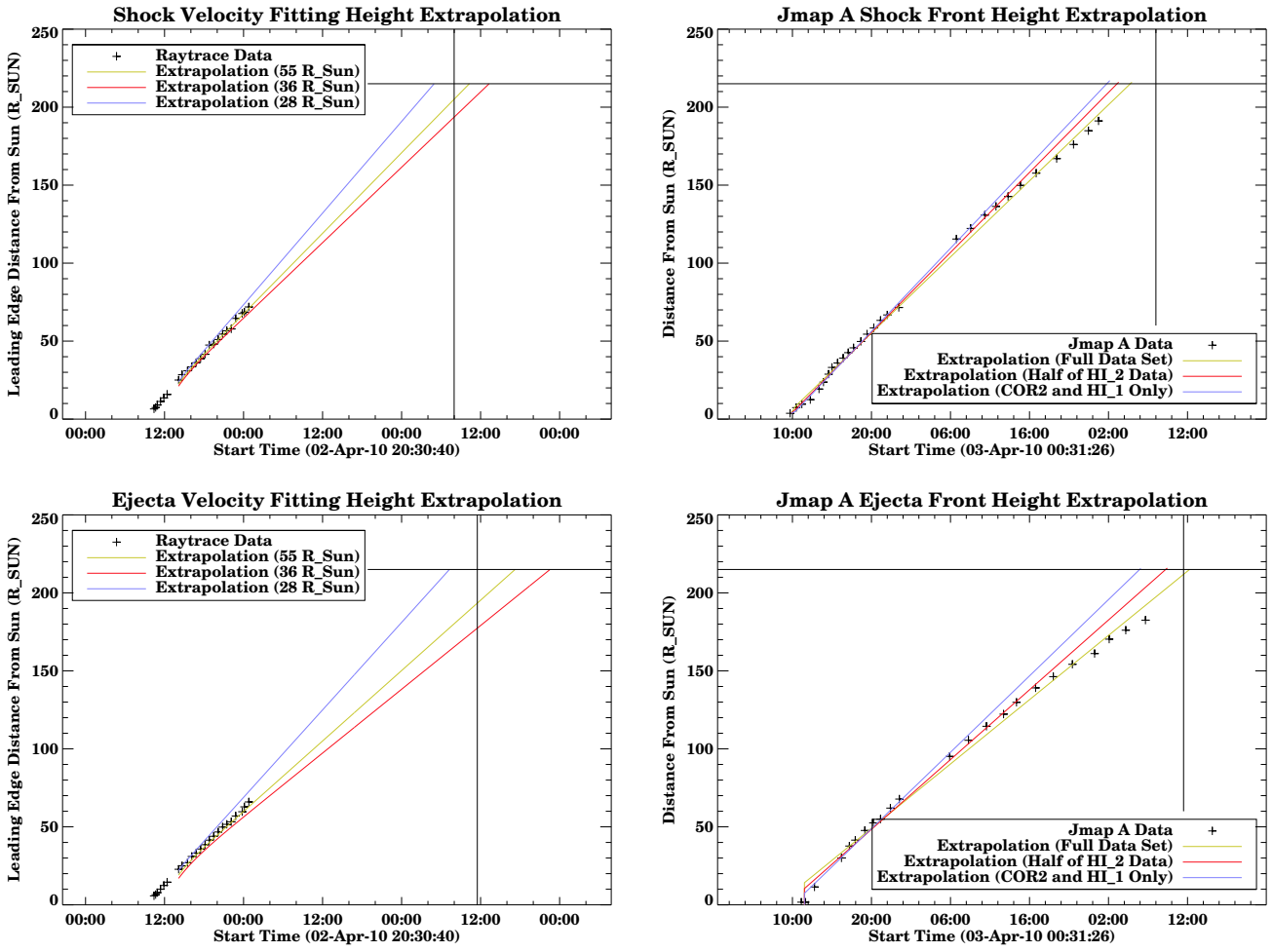

Fig. 8.— Predictions of arrival times for both fronts based on different subsets of each data set. The distances in the raytrace data denote the last measurement used for the extrapolation. The Jmap data is listed with the amount of HI-2 data used in the extrapolation.